

# Double hexagonal close-packed structure revealed in a single colloidal crystal grain by Bragg rod analysis

J.-M. Meijer,<sup>a</sup> A. Shabalin,<sup>b</sup> R. Dronyak,<sup>b</sup> O. M. Yefanov,<sup>b,‡</sup> A. Singer,<sup>b,§</sup> R. P. Kurta,<sup>b</sup> U. Lorenz,<sup>b</sup> O. Gorobstov,<sup>b</sup> D. Dzhigaev,<sup>b,c</sup> J. Gulden,<sup>b,¶</sup> D. V. Byelov,<sup>a</sup> A. V. Zozulya,<sup>b</sup> M. Sprung,<sup>b</sup> I. A. Vartanyants<sup>b,c</sup> and A. V. Petukhov<sup>a\*</sup>

<sup>a</sup>Van 't Hoff Laboratory for Physical and Colloid Chemistry, Utrecht University, Padualaan 8, Utrecht, The Netherlands, <sup>b</sup>Deutsches Elektronen-Synchrotron DESY, Notkestrasse 85, D-22607 Hamburg, Germany, and <sup>c</sup>National Nuclear Research University, 'MEPhI', 115409 Moscow, Russian Federation. Correspondence e-mail: a.v.petukhov@uu.nl

A coherent X-ray diffraction study of a single colloidal crystal grain composed of silica spheres is reported. The diffraction data contain Bragg peaks and additional features in the form of Bragg rods, which are related to the stacking of the hexagonally close-packed layers. The profile of the Bragg rod shows distinct intensity modulations which, under the specific experimental conditions used here, are directly related to the stacking sequence of the layers. Using a model for the scattered intensity along the Bragg rod for an exact stacking sequence of a finite number of hexagonally close-packed layers, it is found that a double hexagonal close-packed stacking sequence is present in the colloidal crystal grain. This analysis method opens up ways to obtain crucial structural information from finite-sized crystalline samples by employing advanced third-generation X-ray sources.

© 2014 International Union of Crystallography

## 1. Introduction

Colloidal crystals and their internal structure have been the focus of many investigations because of their possible application as functional nanomaterials, for instance as photonic crystals (Galisteo-López *et al.*, 2011; Blanco *et al.*, 2000; Vlasov *et al.*, 2001). The presence of defects in the crystal structure influences the functional properties of the colloidal crystal, and therefore it is important to characterize both the crystal and its defect structures in detail.

Characterization of the three-dimensional structure of colloidal crystals can be done in direct or reciprocal space using a number of approaches. Advanced confocal laser scanning microscopy allows imaging of the particle positions in detail, but only small sample volumes can be used owing to limits in resolution and penetration depth (Schall, 2009). Light scattering can provide structural information but has a severely limited  $q$  range [ $q = (4\pi/\lambda)\sin\theta$ , where  $\theta$  is half the scattering angle and  $\lambda$  is the wavelength of the incident radiation]. In addition, for these optical techniques the refractive index mismatch, which is essential for photonic properties, greatly complicates quantitative structure analysis. These problems can be overcome by using X-ray diffraction, which has already been successfully employed for colloidal

crystals. For instance, statistically averaged information about the crystal structure and disorder in macroscopic samples has been revealed in small-angle X-ray diffraction studies (Vos *et al.*, 1997; Versmold *et al.*, 1999; Petukhov *et al.*, 2002, 2003; Hilhorst *et al.*, 2009; Sinitskii *et al.*, 2010; Byelov *et al.*, 2010). Furthermore, recent developments in X-ray techniques have also allowed for novel approaches, such as coherent X-ray diffraction imaging (CXDI) (Gulden *et al.*, 2010, 2012), as well as hard and soft X-ray microscopy (Hilhorst *et al.*, 2012; Bosak *et al.*, 2010; Byelov *et al.*, 2013), which are able to access local structures in colloidal crystals.

Colloidal spheres are known to self-organize into structures consisting of close-packed hexagonal layers that occupy three specific positions (Sloane, 1998). There are two simple regular lattices, the hexagonal close-packed (h.c.p.) and face-centred cubic (f.c.c.) structures. However, because of the small free-energy difference between f.c.c. and h.c.p. (Bolhuis *et al.*, 1997; Bruce *et al.*, 1997; Mau & Huse, 1999), a random mixture of the two stacking types, the so-called random hexagonal close-packed (r.h.c.p.) structure, is often observed (Dolbnya *et al.*, 2005; Zhu *et al.*, 1997; Kegel & Dhont, 2000). In X-ray diffraction, this type of stacking disorder leads to the appearance of Bragg rods along the direction normal to the close-packed hexagonal layers (Versmold *et al.*, 1999; Petukhov *et al.*, 2003).

In this work, we study the Bragg rods observed for a small (about 4  $\mu\text{m}$ ) single colloidal crystal grain using coherent X-ray diffraction. In contrast with previous studies that only

‡ Present address: Centre for Free-Electron Laser Science, DESY, Notkestrasse 85, D-22607 Hamburg, Germany.

§ Present address: University of California, San Diego, CA 92093, USA.

¶ Present address: Fachhochschule Stralsund, Zur Schwedenschanze 15, D-18435 Stralsund, Germany.

collected statistically averaged data over large ( $>100\ \mu\text{m}$ ) sample areas, and hence collected smeared intensities along the Bragg rods, here we observe unusually distinct intensity modulations along the Bragg rod related to the r.h.c.p. stacking sequence. We demonstrate that, under these conditions, we can reveal the specific stacking sequence of layer positions by fitting a simple stacking model for a finite number of hexagonally close-packed layers to the Bragg rod intensity profile. Our analysis reveals the presence of a double hexagonal close-packed (d.h.c.p.) stacking sequence in this particular colloidal crystal grain. This approach enables direct access to structural information of finite-sized objects on the basis of coherent diffraction measurements, without the challenging phase retrieval data analysis typical for CXDI.

## 2. Experiment

The samples were prepared from dried sediments of colloidal crystals that showed characteristic optical Bragg reflections similar to those observed by Gulden *et al.* (2012). The sediments were obtained by drying a colloidal suspension of sterically stabilized silica spheres with a diameter ( $2R$ ) of 230 nm in cyclohexane over several months. Small grains were obtained by mechanically crushing a piece of the ordered sediment. Individual grains were picked up manually using a micromanipulator (PatchMan NP2, Eppendorf) and connected to the tip of a  $10\ \mu\text{m}$ -thick carbon fibre, which was mounted on the sample holder. The colloidal crystal grain used in this study was imaged with light microscopy and determined to have dimensions of about  $2 \times 3 \times 4\ \mu\text{m}$ .

The experiment was performed on the coherence beamline P10 of the PETRA III synchrotron (DESY, 2014). A monochromatic X-ray beam of 8 keV photon energy was focused on the sample at a distance of 87.7 m from the source, using transfocator optics (Zozulya *et al.*, 2012) based on compound refractive lenses (CRLs). The CRL optics were positioned 2.2 m upstream from the sample, and a slit system of  $75 \times 75\ \mu\text{m}$  in size, located 1.5 m before the CRL, was used to select a coherent portion of the beam. The size of the focal spot at the sample position was  $5.5\ \mu\text{m}$  (full width at half-maximum, FWHM) in the horizontal direction and  $3.2\ \mu\text{m}$  (FWHM) in the vertical direction, with about  $10^{11}$  photons  $\text{s}^{-1}$  of total intensity. To inhibit radiation damage, the grain was cryo-cooled with a nitrogen flow. Coherent diffraction patterns were acquired using a MAXIPIX detector (ESRF, Grenoble, France) with  $516 \times 516$  pixels and a pixel size of  $55 \times 55\ \mu\text{m}$ . The detector was located 5.1 m from the sample, with a minimum resolution in reciprocal space of  $0.4372\ \mu\text{m}^{-1}$  defined by the geometry of the experiment and pixel size. An evacuated flight tube was used between the sample and the detector in order to reduce background scattering. A full data set consisted of a rotation series of 360 diffraction patterns with a  $0.5^\circ$  increment, thus covering the entire reciprocal space. At each angular position, a series of 100 diffraction patterns were measured to provide a good signal-to-noise ratio. To access the scattering signal close to the directly transmitted beam, a semi-transparent beamstop made of Si

wafer ( $300\ \mu\text{m}$  thick,  $3 \times 3\ \text{mm}$  in area) was installed in front of the detector. Additionally, a Ta disc of diameter 0.5 mm was glued on top of the Si wafer to absorb the direct beam completely.

## 3. Theoretical model

It is well known that colloidal spheres arrange into a stacking of close-packed hexagonal layers that is similar to atomic crystals, such as metals (Sloane, 1998). In these structures, a sphere in a given layer will be arranged in the hollow site formed by three spheres in the layer below. Since two subsequent layers cannot have the same lateral position, there are only two of these positions in a hexagonally packed layer, resulting in a total of three distinct layer positions, denoted *A*, *B* and *C*. The two simplest periodic stacking sequences of these layers are h.c.p., with an *ABAB...* stacking, and f.c.c., with an *ABCABC...* stacking, as shown in Fig. 1(a). In contrast with their atomic counterparts, colloidal crystals are

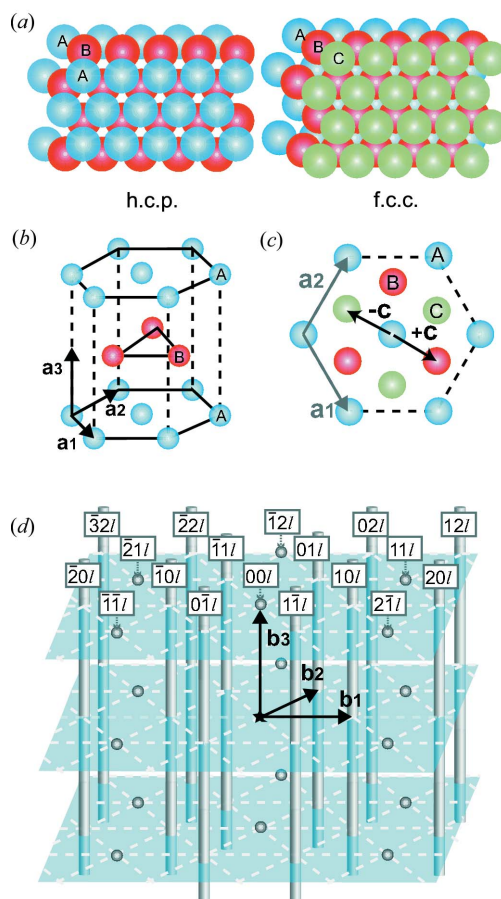


**Figure 1**  
(a) Stacking of close-packed hexagonal layers with an h.c.p. or f.c.c. stacking sequence. (b) The hexagonal unit cell in direct space, together with the basis vectors  $a_1$ ,  $a_2$  and  $a_3$ . (c) A top view of the *A*, *B* and *C* positions and the lateral displacement vector *c*. (d) A sketch of the reciprocal lattice of randomly stacked hexagonally close-packed crystals described by vectors  $b_1$ ,  $b_2$  and  $b_3$ . For specific *hk* indices, as labelled, the intensity along *l* is concentrated into distinct Bragg peaks (grey spheres) for  $h - k$  divisible by 3, and smeared into Bragg rods (grey rods) for  $h - k$  not divisible by 3.

often found to possess an r.h.c.p. stacking, because of the very low energy difference between the two crystal structures of less than  $10^{-3} kT$  per particle (Bolhuis *et al.*, 1997), where  $k$  is the Boltzmann constant,  $1.3806488 \times 10^{-23} \text{ J K}^{-1}$ ). In an RCHP structure, the positions of the hexagonal layers follow a random stacking sequence, causing planar stacking faults in either a pure h.c.p. or a pure f.c.c. crystal structure, and these can be observed by X-ray diffraction (Petukhov *et al.*, 2003; Hilhorst *et al.*, 2009; Byelov *et al.*, 2010). However, there are also other periodic structures that close-packed hexagonal layers can form. In these cases the repeating unit cell is extended over more than three layers. An example of this is the d.h.c.p. structure, with a stacking sequence of *ABCBA*CB... This crystal structure is found for some of the rare earth metals (Pearson, 1967) but has not been reported before for colloidal crystals of spheres.

In this work, we analyse a single colloidal crystal grain consisting of a finite number of close-packed hexagonal layers. To be able to extract the exact r.h.c.p. stacking sequence of the layers, we will describe the structure of colloidal crystals by the hexagonal set of basis vectors  $\mathbf{a}_1$ ,  $\mathbf{a}_2$  and  $\mathbf{a}_3$ , as shown in Fig. 1(b). The hexagonal layers are described by  $\mathbf{a}_1$  and  $\mathbf{a}_2$ , with  $|\mathbf{a}_1| = |\mathbf{a}_2| = a$ , which is the interparticle distance, and the interlayer spacing is described by the vector  $\mathbf{a}_3$ . The layers are stacked along the  $\mathbf{a}_3$  or [001] direction and the order of the A, B or C layer positions, or their respective lateral displacements, determines the stacking sequence. We define the lateral displacements as ‘forward’ (+) for A to B, B to C or C to A, or ‘backward’ (–) for A to C, B to A or C to B. This displacement can be described in plane by the ‘forward’ vector  $\mathbf{c} = (2\mathbf{a}_1/3) + (\mathbf{a}_2/3)$  and the ‘backward’ vector  $-\mathbf{c}$  (see Fig. 1c).

Based on the hexagonal set of direct space basis vectors, the reciprocal basis vectors  $\mathbf{b}_1$ ,  $\mathbf{b}_2$  and  $\mathbf{b}_3$  can be determined in the usual way (Guinier, 1994). The scattering vector  $\mathbf{q}$  is then described by  $\mathbf{q} = h\mathbf{b}_1 + k\mathbf{b}_2 + l\mathbf{b}_3$ . In Fig. 1(d) a schematic representation of the reciprocal space lattice is shown. Here, the blue planes illustrate the hexagonal planes described by  $\mathbf{b}_1$  and  $\mathbf{b}_2$ . Owing to the two-dimensional periodicity inside each hexagonal plane, the scattering intensity in reciprocal space will be concentrated around the integer values of  $h$  and  $k$ . Stacking faults, inherent in an r.h.c.p. structure, break the interlayer periodicity, thus smearing out the diffraction features in rods along  $l$ . The diffraction amplitude of each subsequent layer along  $l$  is dependent on the layer position which, in direct space as described above, will be shifted by the vector  $\mathbf{a}_3$  in the direction normal to the layers and by  $\pm\mathbf{c}$  laterally. Correspondingly, in reciprocal space the contribution of the  $n$ th layer to the diffraction amplitude will receive a  $\mathbf{q}$ -dependent phase shift along  $l$ . This phase shift is described by  $\exp(i\Delta\varphi_n + 2\pi inl)$ , where  $\Delta\varphi_n$  is the phase shift caused by the lateral displacement  $\pm\mathbf{c}$ , given by a recurrent relation

$$\Delta\varphi_n = \Delta\varphi_{n-1} \pm 2\pi \frac{(h-k)}{3}. \quad (1)$$

Using equation (1), the structure factor  $S(l)$  of a crystal containing  $N$  hexagonal layers is given by

$$S(l) = \left| \sum_{n=0}^{N-1} \exp(i\Delta\varphi_n + 2\pi inl) \right|^2. \quad (2)$$

Here, the first layer is  $n = 0$  and always assigned an A position. It must be noted that all layers are assumed to be of the same size. For specific  $hk$  indices such that  $h - k$  is divisible by 3, the phase shift  $\Delta\varphi_n$  is always a multiple of  $2\pi$  and  $S(l)$  reduces to the usual result (Guinier, 1994)

$$S(l) = \left| \frac{\sin(\pi Nl)}{\sin(\pi l)} \right|^2, \quad (3)$$

with well defined Bragg peaks around integer values of  $l$ , independent of the stacking sequence and thus resembling a perfectly regular crystal with  $N$  planes. The positions of the Bragg peaks are represented by the grey spheres in Fig. 1(d) and are regularly spaced along  $l$  at integer values.

For the other  $hk$  indices,  $h - k$  not divisible by 3, the  $S(l)$  profile will depend sensitively on the exact sequence of the  $N$  layers<sup>1</sup> as given by equation (2), and the intensity is concentrated into rods along  $l$  (grey rods in Fig. 1d). For each stacking sequence, a unique  $S(l)$  profile is obtained that is periodic with a period of  $l = 1$ .

Finally, the total scattering intensity  $I(l)$  for a colloidal crystal grain is determined by the equation

$$I(l) = P(l) S(l), \quad (4)$$

where  $P(l)$  is the form factor of a colloidal sphere with radius  $R$  normalized to its volume (Pedersen, 2002):

$$P(l) = \left\{ \frac{3[\sin(qR) - qR \cos(qR)]}{(qR)^3} \right\}^2. \quad (5)$$

Here, the  $q$  values along an  $hkl$  rod are given by

$$q_{hkl} = (q_{hk0}^2 + q_{00l}^2)^{1/2} = \frac{2\pi}{a} \left[ \frac{4}{3}(h^2 + k^2 + hk) + \frac{3}{2}l^2 \right]^{1/2}, \quad (6)$$

where we assume that the interparticle distance  $a$  is 1% larger than the average particle diameter ( $2R$ ), as previously shown for polydisperse colloidal spheres (Petukhov *et al.*, 2006).

It must be noted that the  $P_{hk}(l)$  contribution to  $I(l)$  along  $l$  depends on the  $hk$  indices, while the  $S(l)$  contribution is only dependent on the stacking sequence. Therefore, groups of  $hkl$  rods with the same  $P_{hk}(l)$  contributions can be classified into a general family, for example all rods  $10l$ ,  $01l$ ,  $\bar{1}0l$ ,  $0\bar{1}l$ ,  $\bar{1}1l$  and  $1\bar{1}l$  belong to the  $10l$  family.

#### 4. Results and discussion

In the full  $180^\circ$  coherent X-ray diffraction data set collected from the colloidal crystal grain, a number of Bragg peaks and distinct Bragg rods were observed. The Bragg rods indicate the presence of stacking disorder in the sample. Fig. 2(a) shows a two dimensional diffraction pattern where the 001 Bragg peaks and two  $21l$  Bragg rods (indicated by arrows) are clearly visible. The darker square region in the middle of the

<sup>1</sup> Supporting information for this paper is available from the IUCr electronic archives (Reference: VH5002).

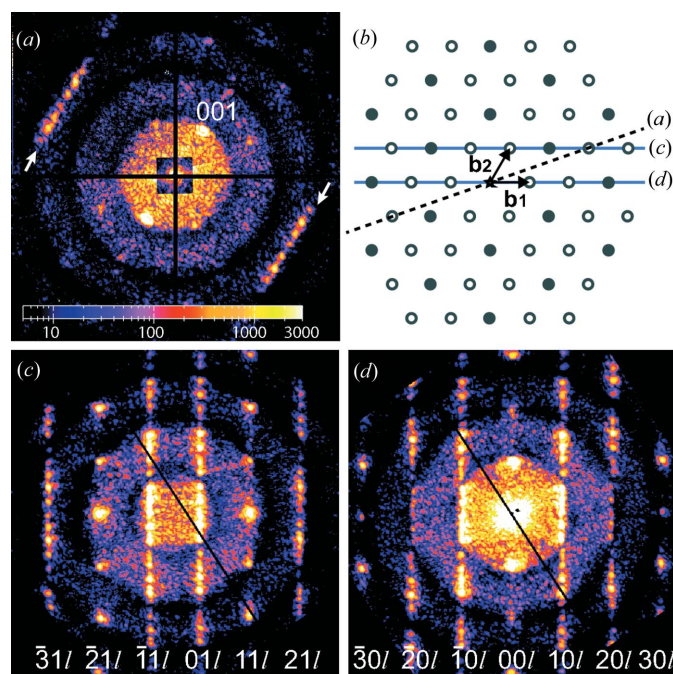


**Figure 2**  
 (a) Two-dimensional diffraction pattern measured along the  $[4\bar{5}0]$  direction of the individual crystal grain, where the 001 Bragg peaks and two Bragg rods of the  $21l$  family are clearly visible (indicated by white arrows). (b) Top view of the reciprocal space lattice along  $l$ . Filled symbols represent Bragg peak positions and open symbols represent Bragg rod positions. The dashed line shows where the Ewald sphere of (a) cuts through the  $21l$  rods. (c) and (d) Two-dimensional slices taken through the full three-dimensional reciprocal space that was constructed from the 360 diffraction patterns. These slices cut through the reciprocal space lattice at the Bragg peak and rod positions illustrated by the blue lines in (b). The slice shown in (c) does not cross through the origin of reciprocal space and therefore does not show the direct beam feature.

diffraction pattern is the area covered by the semi-transparent beam stop, and the zero-intensity crossed lines originate from the gaps separating the four tiles of the MAXIPIX detector. For this sample orientation, the X-ray beam propagates along the  $[4\bar{5}0]$  direction of the colloidal crystal grain and the two  $21l$  Bragg rods lie almost perfectly on the Ewald sphere. This is shown schematically in Fig. 2(b), where the black dashed line indicates the cut through the top view of the reciprocal lattice

(Fig. 1d). Using all 360 diffraction patterns, the full three-dimensional reciprocal space distribution of scattered intensities was constructed. As expected for a crystal with stacking disorder, this revealed the presence of Bragg rods through the three-dimensional reciprocal space and enabled us to extract intensity profiles along all the Bragg rods. Since the coherence length of the beam is larger than our crystal grain and with sufficient detector resolution, we can resolve the fine structure of the Bragg rod. In Figs. 2(c) and 2(d), two extracted two-dimensional slices along  $l$  of the constructed three-dimensional reciprocal space are shown, where the black lines are again due to the detector gaps. The locations of the projections in reciprocal space are indicated by blue lines in the reciprocal lattice shown in Fig. 2(b). In these two-dimensional slices all the specific Bragg rods are labelled and these can be classified as the Bragg rod families  $10l$ ,  $20l$  and  $21l$ . The observed Bragg rods reveal specific modulations of intensity along  $l$ , which are distinctly different from the results reported so far (Vermold *et al.*, 1999; Petukhov *et al.*, 2003; Hilhorst *et al.*, 2009; Byelov *et al.*, 2010; Eliseev *et al.*, 2009). In those studies, much larger colloidal crystals were investigated and the measured Bragg rod profiles, consisting of a smeared intensity distribution between the Bragg peaks, only provide information on the average stacking fault densities.

Bragg rod profiles were extracted from the constructed three-dimensional data set in reciprocal space for the visible Bragg rods, and the  $l$  values were determined by locating the middle of the rod with respect to the centre of the incident beam and scaled with the  $q$  value of the 001 Bragg peak, as this is located at  $l = 1$ . The intensity profiles for the selected Bragg rod families  $10l$ ,  $20l$  and  $21l$  are plotted in Fig. 3, where the intensity modulations can clearly be seen. For each profile, the peak positions are similar while the peak amplitudes differ significantly. This is expected, because for each  $hk$  combination of indices the structure factor  $S(l)$  is the same, while the form factors  $P_{hk}(l)$  are different.

The total number of layers  $N$  in the studied crystal grain was determined by fitting the width of the Bragg peaks along the  $11l$  rod using equation (3) and was found to be 12. The measured  $11l$  rod profile and the corresponding fitting curve, showing good agreement in terms of peak positions and shape, are displayed in Fig. 4. It must be noted that equation (3)

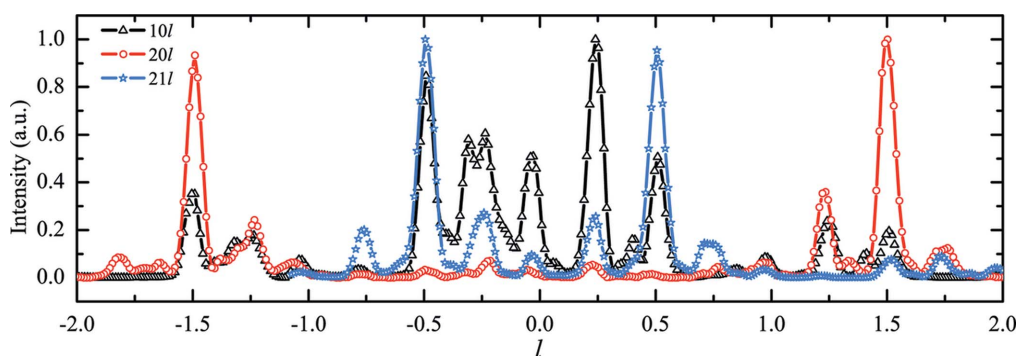


**Figure 3**  
 Normalized experimental Bragg rod profiles of the  $10l$ ,  $20l$  and  $21l$  families (lines + symbols), showing distinct intensity modulations along  $l$ . The peak positions of the families correspond well, while their amplitudes differ because of the different  $P_{hk}(l)$  and  $S(l)$  contributions at the specific  $hk$  indices.

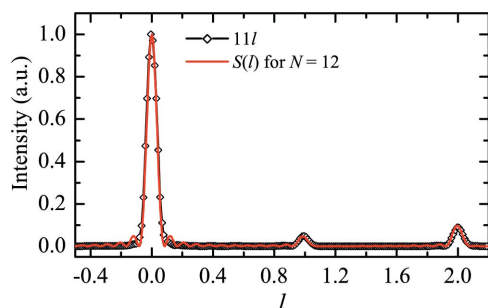


**Figure 4**  
The normalized experimental Bragg peak profile along the  $11l$  direction fitted with a peak model for 12 layers [equation (3)].

assumes that all layers are of the same size. In practice, since the colloidal crystal grain is obtained by fracturing a dried sediment, it is very unlikely that all layers contain the same number of particles. Layers with a smaller size will contribute less to the peak broadening and therefore the actual number  $N$  of layers in the grain might be larger.

Using the model for the intensity distribution  $I(l)$  described by equation (4), the Bragg rod profiles for different stacking sequences of 12 layers were calculated. To obtain quantitative agreement between model and experiment, the intensity over the range  $-1 < l < 1$  was used for analysis, with the exception of the  $20l$  rod, where the range  $0 < l < 2$  was used because of the low intensity.

After careful examination of all possible stacking sequences, we found two sequences containing a d.h.c.p. structure that yielded the best match to the experimental profiles. Fig. 5 shows the experimental Bragg rod profiles for the  $10l$ ,  $20l$  and  $21l$  Bragg rod families, as well as the best fits calculated for the two found d.h.c.p. sequences. The first stacking sequence,  $ABCBA\overline{BCBA}BCB$ , is a perfect d.h.c.p. structure that consists of every second layer at a  $B$  position in an f.c.c. environment and alternating  $A/C$  layers in an h.c.p. environment. The second sequence,  $ABCBA\overline{BCBC}ACB$ , is similar to the first one with the exception of the two underlined layers. These two layers cause a stacking defect in the perfect d.h.c.p. sequence, and change the repeating  $B$  layer to a repeating  $C$  layer. The calculated  $I(l)$  profiles for the two considered d.h.c.p. sequences are very similar in terms of peak

positions, shapes and amplitudes and describe all three experimental Bragg rod profiles very well.

The main difference between the two d.h.c.p. profiles is found periodically at  $l = -0.25, 0.75, 1.75$ , as indicated with arrows in Fig. 5, where a single peak is split into a double peak by the stacking defect. For all three Bragg rod profiles, this is the location where both model profiles deviate from the experimental data. This can be caused by simplifications accepted in the model, such as the assumption that each layer can consist of a different number of particles or the layers can exhibit in-plane stacking disorder (Meijer *et al.*, 2007). In the latter case, two stacking positions are present inside a single h.c.p. layer, such as islands of  $A$  and  $C$  layers coexisting on top of a  $B$  layer. The result is two different stacking sequences in a single grain that will influence  $S(l)$ . The other small deviations between the experimental data and the model could be explained by our simplified approach to determining  $I(l)$ .

The overall good agreement obtained using the simple model for  $I(l)$  shows that the d.h.c.p. structure is the dominant packing arrangement of the colloidal spheres present in the studied crystal grain. This is a remarkable result because the d.h.c.p. structure has not been observed before in colloidal crystals of spheres. Previous studies have indicated that the growth of a sedimentary crystal with an r.h.c.p. structure probably occurs *via* the sequential nucleation of hexagonal layers (Meijer *et al.*, 2007). The interactions are limited to neighbouring layers and, therefore, the d.h.c.p. structure could be just one of the many random coincidental realizations of the r.h.c.p. structure. Alternatively, it could be an effect of the drying process, in which capillary forces of significant strength act on the colloids (Denkov *et al.*, 1992).

### 5. Conclusions and outlook

In the coherent X-ray diffraction data of a single colloidal crystal grain, distinct Bragg peaks and Bragg rods were observed. Characteristic intensity modulations along the Bragg rods indicated the presence of stacking faults in the sequence of close-packed hexagonal layers. The intensity fluctuations are described by a model that takes into account the stacking sequence of a finite number of close-packed hexagonal layers. Using the model, two stacking sequences of

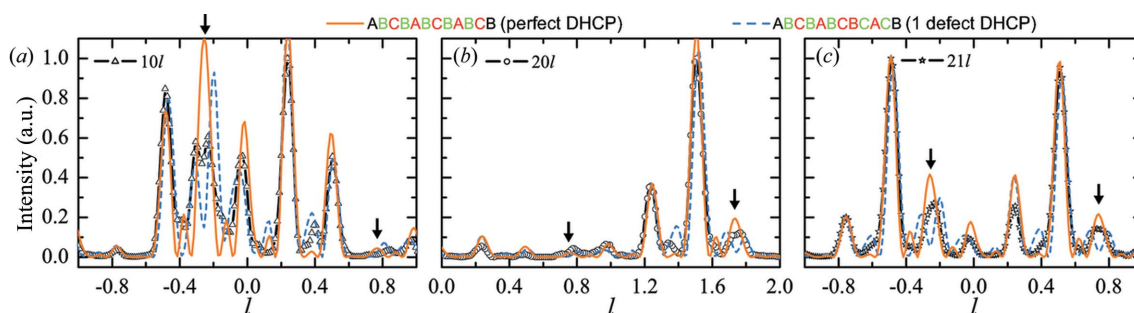


**Figure 5**  
Normalized experimental Bragg rod profiles (black lines + symbols) for (a) the  $10l$ , (b) the  $20l$  and (c) the  $21l$  families, and modelled profiles for two d.h.c.p. structures, a perfect sequence (orange lines) and a sequence with a single stacking fault (blue dashed lines). The specific layer sequence is represented by the  $A$ ,  $B$  and  $C$  sequences (given along the top), where each layer can be in either an h.c.p. environment (red) or an f.c.c. environment (green). Arrows indicate the region where the two d.h.c.p. model profiles mismatch the most and have a single or double peak, respectively.

the d.h.c.p. type, where f.c.c. and h.c.p. stackings alternate periodically, were found to match the experimental data. The slight mismatch between a perfect d.h.c.p. and a single stacking fault d.h.c.p. structure and the experimental data suggests that the grain may contain a stacking fault in a predominantly d.h.c.p. structure. The presence of a d.h.c.p. structure is remarkable as it has not been observed for a colloidal crystal of spheres before.

Although we have taken a relatively simple approach for the analysis of the stacking sequence, our conclusions are consistent with the preliminary results of our independent analysis of three-dimensional electron-density distribution in real space, obtained using a phase retrieval algorithm (Shabalin *et al.*, 2014). With this method, the positions of the individual colloidal particles are determined and, by analysing the projection on one of the crystallographic directions, the stacking sequence can be determined. This agreement shows that our method is a feasible new route for the analysis of finite-sized objects. The proposed method can be applied to more general classes of finite-sized structures studied with high-brilliance third-generation synchrotron sources to extract crucial structure information from the diffraction data.

J. Hilhorst is acknowledged for useful discussions. The P10 beamline team is thanked for providing technical support. DESY is acknowledged for allocating the beamtime. Part of this work was supported by BMBF Proposal 05K10CHG, ‘Coherent Diffraction Imaging and Scattering of Ultrashort Coherent Pulses with Matter’, in the framework of the German–Russian collaboration ‘Development and Use of Accelerator-Based Photon Sources’, and by the Virtual Institute VH-VI-403 of the Helmholtz Association.

## References

- Blanco, A., Chomski, E., Grabtchak, S., Ibisate, M., John, S., Leonard, S. W., Lopez, C., Meseguer, F., Miguez, H., Mondia, J. P., Ozin, G. A., Toader, O. & van Driel, H. M. (2000). *Nature*, **405**, 437–440.
- Bolhuis, P. G., Frenkel, D., Mau, S. C. & Huse, D. A. (1997). *Nature*, **388**, 235–236.
- Bosak, A., Snigireva, I., Napolskii, K. S. & Snigirev, A. (2010). *Adv. Mater.* **22**, 3256–3259.
- Bruce, A., Wilding, N. & Ackland, G. (1997). *Phys. Rev. Lett.* **79**, 3002–3005.
- Byelov, D. V., Hilhorst, J., Leferink op Reinink, A. B., Snigireva, I., Snigirev, A., Vaughan, G. B., Portale, G. & Petukhov, A. V. (2010). *Phase Transitions*, **83**, 107–114.
- Byelov, D. V., Meijer, J., Snigireva, I., Snigirev, A., Rossi, L., van den Pol, E., Kuijk, A., Philipse, A., Imhof, A., van Blaaderen, A., Vroege, G. J. & Petukhov, A. V. (2013). *RSC Adv.* **3**, 15670.
- DESY (2014). *P10 Coherence Applications Beamline*, [http://photon-science.desy.de/facilities/petra\\_iii/beamlines/p10\\_coherence\\_applications/index\\_eng.html](http://photon-science.desy.de/facilities/petra_iii/beamlines/p10_coherence_applications/index_eng.html).
- Denkov, N., Velev, O., Kralchevski, P., Ivanov, I., Yoshimura, H. & Nagayama, K. (1992). *Langmuir*, **8**, 3183–3190.
- Dolbnya, I. P., Petukhov, A. V., Aarts, D. G. A. L., Vroege, G. J. & Lekkerkerker, H. N. W. (2005). *Europhys. Lett.* **72**, 962–968.
- Eliseev, A. A. *et al.* (2009). *JETP Lett.* **90**, 272–277.
- Galisteo-López, J. F., Ibisate, M., Sapienza, R., Froufe-Pérez, L. S., Blanco, A. & López, C. (2011). *Adv. Mater.* **23**, 30–69.
- Guinier, A. (1994). *X-ray Diffraction in Crystals, Imperfect Crystals, and Amorphous Bodies*. New York: Dover Publications Inc.
- Gulden, J., Yefanov, O. M., Mancuso, A. P., Abramova, V. V., Hilhorst, J., Byelov, D., Snigireva, I., Snigirev, A., Petukhov, A. V. & Vartanyants, I. A. (2010). *Phys. Rev. B*, **81**, 224105.
- Gulden, J., Yefanov, O. M., Mancuso, A. P., Dronyak, R., Singer, A., Bernátová, V., Burkhardt, A., Polozhentsev, O., Soldatov, A., Sprung, M. & Vartanyants, I. A. (2012). *Opt. Express*, **20**, 4039–4049.
- Hilhorst, J. *et al.* (2009). *Langmuir*, **25**, 10408–10412.
- Hilhorst, J., van Schooneveld, M. M., Wang, J., de Smit, E., Tyliczszak, T., Raabe, J., Hitchcock, A. P., Obst, M., de Groot, F. M. & Petukhov, A. V. (2012). *Langmuir*, **28**, 3614–3620.
- Kegel, W. K. & Dhont, J. K. G. (2000). *J. Chem. Phys.* **112**, 3431–3436.
- Mau, S. & Huse, D. (1999). *Phys. Rev. E*, **59**, 4396–4401.
- Meijer, J. M., Villeneuve, V. W. & Petukhov, A. V. (2007). *Langmuir*, **23**, 3554–3560.
- Pearson, W. B. (1967). *Handbook of Lattice Spacings and Structure of Metals*. Oxford: Pergamon Press.
- Pedersen, J. S. (2002). *Modeling of Small-Angle Scattering Data from Colloids and Polymer Systems. Neutrons, X-rays and Light: Scattering Methods Applied to Soft Condensed Matter*, edited by P. Linder & Th. Zemb, pp. 391–420. Amsterdam: Elsevier Science.
- Petukhov, A. V., Aarts, D. G. A. L., Dolbnya, I. P., de Hoog, E. H. A., Kassapidou, K., Vroege, G. J., Bras, W. & Lekkerkerker, H. N. W. (2002). *Phys. Rev. Lett.* **88**, 208301.
- Petukhov, A. V., Dolbnya, I. P., Aarts, D. G., Vroege, G. J. & Lekkerkerker, H. N. (2003). *Phys. Rev. Lett.* **90**, 028304.
- Petukhov, A. V., Thijssen, J. H. J., Hart, D. C. 't, Imhof, A., van Blaaderen, A., Dolbnya, I. P., Snigirev, A., Moussaïd, A. & Snigireva, I. (2006). *J. Appl. Cryst.* **39**, 137–144.
- Schall, P. (2009). *Rep. Prog. Phys.* **72**, 076601.
- Shabalin, A. *et al.* (2014). In preparation.
- Sinitskii, A., Abramova, V., Grigorieva, N., Grigoriev, S., Snigirev, A., Byelov, D. V. & Petukhov, A. V. (2010). *EPL*, **89**, 14002.
- Sloane, N. J. A. (1998). *Nature*, **395**, 435–436.
- Versmold, H., Musa, S., Dux, C. & Lindner, P. (1999). *Langmuir*, **15**, 5065–5067.
- Vlasov, Y. A., Bo, X. Z., Sturm, J. C. & Norris, D. J. (2001). *Nature*, **414**, 289–293.
- Vos, W. L., Megens, M., van Kats, C. M. & Bösecke, P. (1997). *Langmuir*, **13**, 6004–6008.
- Zhu, J., Li, M., Rogers, R., Meyer, W., Ottewill, R., Russell, W. & Chaikin, P. (1997). *Nature*, **387**, 883–885.
- Zozulya, A. V., Bondarenko, S., Schavkan, A., Westermeier, F., Grübel, G. & Sprung, M. (2012). *Opt. Express*, **20**, 18967–18976.